Precise measurement of the lattice spacing of LaB_6 standard powder by the x-ray extended range technique using synchrotron radiation

C. T. Chantler,[1] C. Q. Tran,[1] and D. J. Cookson[2]
[1]*School of Physics, University of Melbourne, Victoria 3010, Australia*
[2]*ANSTO, Private Mail Bag 1, Menai, New South Wales 2234, Australia*
and Chem-Mat-CARS-CAT (Sector 15, Building 434D), Argonne National Laboratory, 9700 South Cass Avenue, Argonne, Illinois 6043, USA
(Received 7 December 2003; published 5 April 2004)

We used the basis of the x-ray extended range technique to measure the lattice spacing of LaB_6 standard powder samples relative to silicon 640*b* standard powder samples with an accuracy of 5×10^{-5} Å. Measurements were not constrained to one energy but were carried out over a 5 keV−20 keV energy range. These measurements used powder diffraction to determine the synchrotron beam energy, to diagnose discrepancies in the nominal calibrated beam energies, and to determine beam energy bandwidths as a function of energy. More specifically, this technique is able to yield a result independent of certain energy-dependent systematics and to yield the most accurate determination of the lattice spacing of NIST SRM 660 LaB_6 standard powder so far undertaken. This has direct application to beam line energy calibration, structural evaluation, edge energy calibration, and lattice spacing determinations.

DOI: 10.1103/PhysRevA.69.042101 PACS number(s): 06.20.−f, 32.80.Cy, 42.72.−g, 07.85.Qe

I. INTRODUCTION

Powder diffraction is a widespread technique in physical, chemical, and biological investigations to determine structures and lattice spacings of crystals which cannot be grown large enough even for the most intense current synchrotron x-ray sources. Microcrystalline organic and inorganic samples are synthesized and rapidly analyzed at synchrotron beam lines designed for this purpose. The ability to reliably determine the lattice spacing and index the reflections has generally depended upon standard powder samples produced in different standard laboratories around the world [1,2].

While structures can often be reliably determined directly from the diffraction patterns using Rietveld and other methods, resulting errors often depend upon the errors of calibrating standards used in the measurement. Key questions remaining in the literature relate to the physical meaning (or accuracy) of imputed powder lattice strain and size distribution parameters used in Rietveld analysis, and in the consequent variation of relative intensities with average powder crystallite size and shape. Rapid spinning of the powder inserted into a capillary in the synchrotron beam allows the crystallites to satisfy the Bragg condition, which is a one-dimensional averaging over possible preferred orientations, and hence provides a statistical averaging over crystallite orientations [3]. This allows enough time to collect data on suitable efficient image plates covering angular ranges, or by using integrating point or imaging detectors such as scintillators or charge-coupled device detectors [4,5].

Another key question has related to the value of large flat crystal refractive index corrections when applied to a microcrystalline powder [6]. In general these questions have been inconclusively answered, in part because of inconsistency between results of different powder investigations and the corresponding inconsistency between the results using different reference standards.

The best documented and most widely used powder-diffraction standards for current research have been developed and supplied by the National Institute of Standards and Technology (NIST) including especially the silicon 640 powder standard series, the LaB_6 660 standard series, and the mica 675 (fluorophlogopite) standard. Data on tungsten and silver powders are available although in the absence of a well defined and maintained standard for these powders. Other samples from other sources have been used as internal or instrumental standards, but the essential steps in the propagation of any powder lattice parameter standard have depended on the accurate determination and maintenance of the Si and LaB_6 standards.

In a series of critical experiments [7,8] we employed these two standards and the corresponding quoted lattice parameters to determine the synchrotron x-ray beam energies across wide ranges of energy from 5 keV to 20 keV with an accuracy reaching 0.4 eV. This used the x-ray extended range technique [9,10] to determine the absolute attenuation coefficient of elemental samples, and derived accurate energies from the powder-diffraction peaks. A key element of this technique in the current context is to collect and analyze diffraction patterns over large angular and energy ranges to isolate and correct for a series of systematics often neglected in other methods for energy determination. This approach corrected the nominal beam energies by up to 100 eV or more, allowing more careful interpretation of the experimental results. The high accuracy of this technique in determining the energy of the incident synchrotron beam allows a quantitative measurement of the lattice spacing of the LaB_6 powder standard by direct comparison with the Si 640*b* powder standard.

Two experiments are combined in the analysis of this paper. One experiment on silicon mass attenuation measured the energies of the incident beam at 16 energies between 5 keV and 20 keV. A second experiment on copper mass

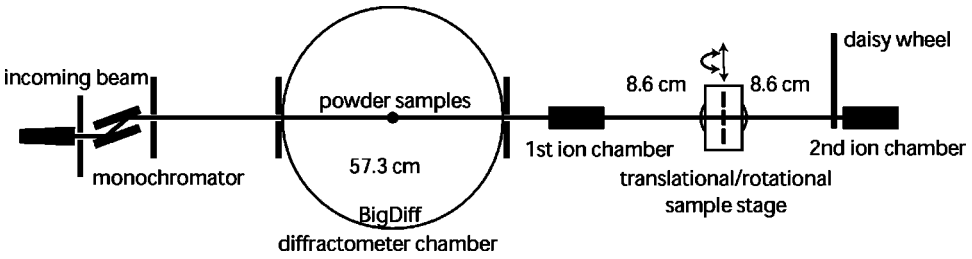

FIG. 1. Experimental layout: copper experiment from 8.85 keV to 20 keV and silicon experiment from 5 keV to 20 keV, conducted at the Photon Factory beamline 20B, Tsukuba, Japan.

attenuation involved determination of the energy by powder diffraction at 11 points covering the energy range between 8.85 keV and 20 keV. Both experimental determinations were calibrated to the monochromator (encoder) angle setting over the full range of the experiment.

II. POWDER DIFFRACTION FOR ENERGY MEASUREMENT

Common methods of measuring the energy of x-ray beams include the use of powder diffraction, single-crystal diffraction, absorption edges, or the use of calibrated energy dispersive detectors. The use of energy dispersive detectors in synchrotron environments is limited due to their narrow dynamic range, significant dead-time correction, and pileup processes. The use of absorption-edge energies as references to calibrate the incident photon energy also has several disadvantages. Edge structures are not well defined and depend on the chemical state of the sample, the energy spread of the incident beam, and the beam divergence. Also, the availability of edge energies is limited.

The powder- and single-crystal diffraction methods are both suitable in the intermediate energy region. The samples are well calibrated and can be used to measure arbitrary energies with good precision and in an affordable time. For higher energies, single-crystal diffraction methods provide higher diffraction intensity. In general a highly accurate single crystal of silicon or germanium can provide the most accurate determination of energy **(**$d(220,\mathrm{Si}) = 0.192\,015\,570(6) \times 10^{-9}$ m, Refs. [11,12]**)**. Form factors [13,14], structure factors, and hence relative intensities can all be determined in a consistent manner. Silicon powder standards and other powder standards have a less accurate lattice spacing determination by perhaps an order of magnitude or more, but still offer an accuracy equivalent to 2 ppm (parts per million) which is fully adequate for many applications. Additionally, suitable powder standards often have a much greater collection efficiency than single crystals, in the appropriate geometries, and for use as a reference or internal standard for experiments involving powders a powder standard is often crucial. Over the 5 keV–20 keV energy range, powder-diffraction methods are well suited to energy determination and structural evaluation given appropriate techniques and standards.

Figure 1 shows the general features of our experimental arrangements for the measurement of mass attenuation of copper from 8.85 keV to 20 keV and for silicon from 5 keV to 20 keV at the Australian National Beamline Facility (ANBF), Photon Factory Synchrotron beamline 20B, Japan.

At ANBF, the incident beam was monochromatized by double reflection from a silicon monochromator which could be detuned to minimize the harmonic components and optimize the throughput [15]. The monochromatized beam was then collimated by a set of slits which defined the beam size to $\approx 1 \times 1$ mm^2 with a vertical divergence of 0.12 ± 0.03 mrad.

The collimating system was followed by a powder diffractometer ("BigDiff" [16,17]) in which the standard powder specimens Si NIST SRM 640*b* **(**$a_0 = 5.430\,940(11)$ Å [1]**)** and LaB_6 NIST SRM 660 **(**$a_0 = 4.15\,695(6)$ Å [1]**)** were used (unsorted as to particle size) to determine the energy of the x rays. Six (20×40 cm^2) image plates of 100 μm (0.01° equivalent) resolution mounted in the diffractometer at 0.57 m radius covered an angular range from −120° to 120° [18]. The angular positions of these image plates were determined from the positions of a set of fiducial marks provided by radioactive sources embedded in the perimeter of the diffractometer.

III. THE X-RAY EXTENDED RANGE TECHNIQUE (XERT) IN THE CONTEXT OF POWDER MEASUREMENTS

There are several sources of systematic errors involved in a powder-diffraction measurement, which are functions of the beam energy and diffraction angle. The XERT involves carrying out measurements over extended ranges of energy and angle. The extended set of data obtained is able to quantify these systematics and as a consequence provide a more accurate characterization of the incident beam.

Numerous systematics have been addressed in these experiments. For example, energies were observed to drift with the encoder reading of the monochromator over time after the monochromator was moved to any particular energy setting. The magnitude of this drift varied from 0 eV to 1.5 eV, but was typically 0.5 eV over a few minutes (Fig. 2). In most cases this was seen to have settled to within 0.1 eV of a stable value within about 5 min. This settling time was allowed for before making the energy measurements. Powder-diffraction patterns required exposures from a few minutes to ≈30 min depending upon the energy and hence upon the diffraction peak strengths and the powder transparencies.

Peak positions of the lines were determined by a nonlinear least-squares fit of the actual data using Lorentzian profiles with either a slowly varying or constant background.

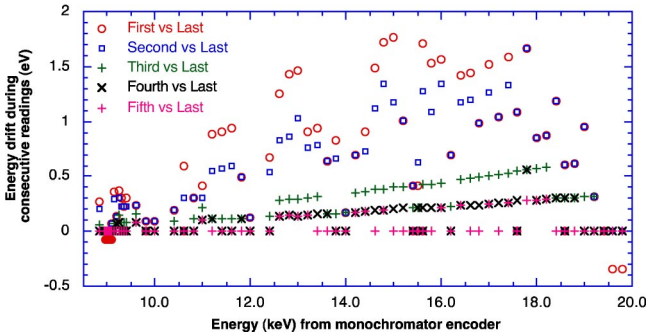

FIG. 2. Drifts of the monochromator encoder setting corresponding to energy drifts of the order of 0.5 eV–1.5 eV are observed during a few minutes after changing (stepping) the energy. Encoder settings are referred to later encoder settings with readings separated by approximately 1 min. Settling times were allowed for this prior to the direct energy measurements.

Several other asymmetric and symmetric profile shapes have been used in past literature but the error of this approach for this data is minor, as the peak profiles have similar shapes for both powders.

Rietveld methods constrain individual relative intensities of different peaks and may confirm relative widths. We note that powder relative intensities are not historically well fitted without large corrections for roughness and size distribution parameters. Systematic centroid errors due to constraints caused by fitting intensities according to an inadequate model, introduced in Rietveld analysis, may exceed any gain compared to simply avoiding the constraints by fitting directly for the lattice spacing (or energy). Peaks in 2θ were determined with precisions [one standard deviation (1sd)] of roughly 0.0001°-0.001°. Reduced χ_r^2 values were generally reasonable and varied from 1 to 20. Some of this mismatch was indeed due to inadequacy of the fitting profile (at this level), and to experimental apparent noise; which in turn can affect the determined centroid. Therefore reported errors are the fitted uncertainty scaled by χ_r^2, i.e., $\sigma_{peak}=\sigma_{1sd}\sqrt{\chi_r^2}$.

IV. POWDER CALIBRATION TO DIAGNOSE THE SYNCHROTRON MONOCHROMATED BEAM DIVERGENCE AND MONOCHROMATICITY

The widths of the powder-diffraction peaks were investigated to confirm their consistency with the image plate resolution, capillary dimension, powder transparency, and beam divergence and bandwidth. Widths varied from close to the image plate resolution limit (0.01° [19]) to typically 0.07° or so (particularly for the lowest order, strongest reflection, or for the highest angle reflections). Fitting precision for widths was generally good and varied from extremes of ≈0.000 01° to ≈0.01° after allowance for $\sqrt{\chi_r^2}$. Typically the uncertainties were of order 0.0001°–0.001°.

Although Rietveld analysis was not used for reasons provided above, the logic and functional form of the observed widths was investigated. The vertical divergence of the x-ray beam results in a broadening of the powder-diffraction lines, similar to the broadening due to the energy window ΔE.

The observed linewidths of the diffraction peaks depend on contributions from several factors: the divergence of the incident beam δ_{div}, the energy window of the incident beam ΔE, the linewidth of the rocking curve of the powder sample δ_s, the size of the powder sample δ_{sz}, the absorption of the powder sample, and the detector resolution δ_{det}. The beam divergence δ_{div} depends on the geometry of the experimental arrangement only, and in our energy measurement the vertical component of the beam divergence dominates over the horizontal component.

To first order (in a Gaussian approximation) all factors mentioned above are independent of each other and the observed linewidths add these contributions in quadrature:

$$\delta\theta_{obs}^2 = \delta_{sz}^2 + \delta_{div}^2 + \delta_{det}^2 + \delta_E(\theta)^2 + \delta_s(\theta)^2. \tag{1}$$

However, the first three terms are of the same order: $\delta_{sz} \approx \tan^{-1}[0.1\ \text{mm}/R\ (R=\text{source to detector distance})] \approx 0.01°$, $\delta_{div} \approx 0.007°$, and $\delta_{det} \approx 0.01°$. $\delta_E(\theta)$ and $\delta_s(\theta)$ have significant dependencies upon θ and E. $\delta_s(\theta)$ can be significant compared to the other factors for the lowest-order reflection(s), where the diffraction width might reach 0.004° or more; but for higher-order reflections the diffraction width (as opposed to the geometrical broadening) is usually negligible at only a few arcseconds. From Bragg's law we have

$$\delta_E(\theta) = \frac{\Delta E}{E}\tan(\theta). \tag{2}$$

The broadening due to the bandpass $\delta_E(\theta)$ gets significantly larger with angle and rapidly dominates over all the other contributions. Therefore, if we plot $\delta\theta_{obs}^2$ as a function of $(\tan^2\theta)$, then the energy bandpass of the monochromated incident beam can be obtained from the slope of the plot. Note that in powder research a different dependence of full width at half 20 maximum is cited [20] of the form

$$\delta\theta_{obs} = A/\cos\ \theta + B\ \tan\ \theta, \tag{3}$$

where A and B are interpreted to relate to crystal size and microstrain, respectively. This is not a unique physical interpretation, implying that the parameters derived from such an investigation may have little physical meaning. Further, this form does not appear to match the current data in any manner. Therefore, either these effects are absent in our case or the physical model is inappropriate.

The y intercept includes the intrinsic divergence of the beam δ_{div}, the source size δ_{sz}, and the detector resolution δ_{det}. Because several components are of the same magnitude, the profile shapes are important and in general the convolved linewidth is significantly less than the quadrature sum:

$$\delta\theta_{obs}^2 \simeq \delta_{y0}^2 + \delta_E(\theta)^2 + \delta_s(\theta)^2, \quad \delta_{y0}^2 \ll \delta_{sz}^2 + \delta_{div}^2 + \delta_{det}^2,$$

$$\delta_{y0}^2 > \max(\delta_{sz}^2, \delta_{div}^2, \delta_{det}^2). \tag{4}$$

Figure 3 shows a typical plot at 10 keV. This shows the general consistency of the profile width dependence upon angle. A small discrepancy at low diffraction angles is a result of a misalignment of the system.

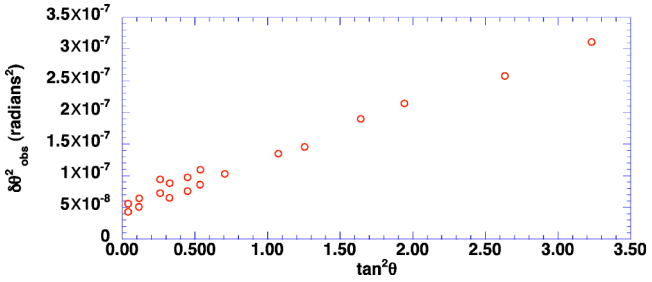

FIG. 3. Linear dependence of $\delta\theta^2_{obs}$ vs $\tan^2\theta$ for a synchrotron beam energy of 10 keV [see Eq. (2)]. The slope represents the energy window $\Delta E/E$ and the y intercept gives the convolved width of the beam divergence, source size, and detector resolution (in this case, $\approx 0.02°$). Error bars are approximately the size of the circle.

The relative energy bandpass $\Delta E/E$ as shown in Fig. 4 increases with energy. This increase follows Bragg's law applied to quantify the energy bandpass of the monochromator for a particular lattice plane:

$$\delta_E(\theta) = \frac{\Delta E}{\delta d_{mono}} \delta d_{mono} + \frac{\Delta E}{\delta \theta_{mono}} \delta\theta_{mono}, \tag{5}$$

therefore

$$\Delta E/E = \delta d_{mono}/d_{mono} + \cot\ \theta_{mono} \delta\theta_{mono}. \tag{6}$$

At higher energies, the Bragg angles at the monochromator θ_{mono} decrease leading to an increase in the energy window of the incident beam $\Delta E/E$. In all cases the linewidths were consistent with a convolution of widths due to the vertical divergence, the monochromator bandpass, the sample width in the beam, and the image plate reader resolution. The clarity of these physical trends indicates both the quality and consistency of the data.

This in turn allowed the determination of the energy bandwidth or the degree of monochromaticity of the x-ray beam. Final estimates from experimental energy bandwidths varied between 1.6 eV (full width at half maximum) and almost 9 eV for the highest 20 keV energies.

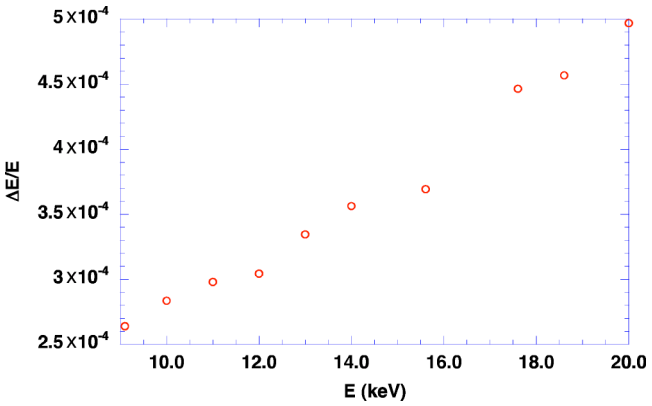

FIG. 4. Energy bandpass $\Delta E/E$ vs energy E. The increase in $\Delta E/E$ as a function of energy E is in agreement with the prediction of Eq. (6).

V. CONSISTENCY OF POWDER-DIFFRACTION ENERGY DETERMINATIONS AND RECALIBRATION OF SYNCHROTRON BEAM LINE MONOCHROMATION

Each image plate must be corrected for a constant offset of the recorded angular 2θ positions (in other words, a slight misalignment of the radioactive fiducials used to determine the plate locations) of up to 0.04° or 400 μm, or equivalent to $\approx$10 eV–30 eV. These corrections are consistent for the set of all (say 10–20) exposures taken with the same image plate, as expected. A linear fitting model was therefore applied using a constant offset in the angular positions of the powder lines for each image plate, to locate the predefined positions of the radioactive fiducials on an absolute scale. In other words $\theta = \theta_{meas} + \delta\theta_{offset,plate\ k}$. As a consequence, the defining equation can be written as

$$\theta_{meas} = \arcsin\left(\frac{hc}{2E_i a_0}\sqrt{h_j + k_j + l_j}\right) - \delta\theta_{offset,plate\ k}. \tag{7}$$

This equation can be linearized to give a more convenient form for least-squares fitting:

$$\sin\ \theta \approx \sin\ \theta_{meas} + \delta\theta_{offset,plate\ k} \cos\ \theta_{meas} \tag{8}$$

and therefore the fitted energies can be calculated from the y intercept of the fitted line:

$$y(E_i, \theta_{meas_j}, \delta\theta_{offset,plate\ k}) = \left(\frac{\sin\ \theta_{meas_j}}{\sqrt{h_j + k_j + l_j}}\right) = \frac{hc}{2a_0 E_i} - \delta\theta_{offset,plate\ k}\frac{\cos\ \theta_{meas_j}}{\sqrt{h_j + k_j + l_j}}. \tag{9}$$

The results for the copper experimental energy determinations using the Si 640*b* and LaB_6 660 powder standards are shown in Table I. Fitted uncertainties matched the variation observed between fits, indicating that the computation was robust and self-consistent.

The results for the silicon experimental energy determination over 16 energies using the Si 640*b* and LaB_6 660 powder standards are summarized and compared in Table II. There were repeated measurements at 8 keV and 10 keV for testing the self-consistency of the measurements. The measurement at 5 keV using Si 640*b* was not useful due to the large air and sample absorption at this low energy.

A separate test was made using fits of individual image plates to assess the self-consistency of local results with the final averages, and to identify any possible outliers. The results of this fit show insignificant differences compared to those of the fits of all plates in Table I. The resultant energies obtained with the two powder standards were averaged with the weighting derived from the corresponding errors.

Energies from both powder determinations were highly consistent and determined corrections to the nominal energy settings of the monochromator of 20 eV–110 eV (Figs. 5 and 6). For a well-determined energy (e.g., 10 keV) in each experiment the determinations corresponded to a mean $|\Delta\theta| = 0.000\ 40° - 0.000\ 48°$, for some 17–77 measured peaks.

TABLE I. Energy calibration using Si 640*b* and LaB_6 powder standards for the energies used with copper attenuation samples. The nominal energies (E_{nom}) at which the calibrations were conducted are compared with the calibrated energies using Si 640*b* ($E_{cal,Si}$) and LaB_6 (E_{cal,LaB_6}). $\sigma_{E_{cal,Si}}$ and $\sigma_{E_{cal,LaB_6}}$ are the 1 sd uncertainties corresponding to $E_{cal,Si}$ and E_{cal,LaB_6}, respectively. $E_{LaB_6}-E_{Si}$ is the difference in eV between the determined energies, with the corresponding σ given. Note that the difference is of a consistent sign and magnitude. The calibrated energies using the Si 640*b* and LaB_6 660 powder standards were consistent within the cited uncertainties.

E_{nom} (eV)	$E_{cal,Si}$ (eV)	$\sigma_{E_{cal,Si}}$ (eV)	E_{cal,LaB_6} (eV)	$\sigma_{E_{cal,LaB_6}}$ (eV)	$E_{LaB_6}-E_{Si}$ (eV)	$\sigma_{E_{LaB6_6}-E_{Si}}$ (eV)
20000	20027.9	0.55	20029.6	0.62	1.70	0.83
18600	18704.3	0.61	18706.0	0.47	1.70	0.78
17600	17695.9	0.59	17697.2	0.51	1.30	0.78
15600	15676.2	0.36	15677.6	0.39	1.40	0.53
14000	14063.8	0.40	14065.9	0.30	2.10	0.50
13000	13057.5	0.45	13058.8	0.26	1.30	0.52
12000	12050.0	0.37	12051.5	0.26	1.50	0.45
11000	11042.9	0.39	11043.3	0.16	0.40	0.42
10000	10038.6	1.23	10036.1	0.19	−2.50	1.25
9100	9132.2	0.40	9132.8	0.35	0.59	0.53
8950	8981.7	0.38	8982.8	0.35	1.12	0.51

The uncertainty of these corrected energy values varied from 0.34 eV to 2.4 eV in the silicon experiment (or energy determinations from 28 ppm to 350 ppm). The copper experiment determined weighted mean energies with one standard deviation $\sigma=0.14$ eV–1.0 eV (or energy determinations from 13 ppm to 72 ppm). Resulting accuracies were limited at low energies by air attenuation (as reflected in the error bars) resulting in few and weak peaks on each plate and at the higher energies by the difficulty of uniquely determining the indices of many closely spaced and weak peaks at very high angles.

While relative energy measurements to within about 1 eV have often been achieved, absolute energy determinations may remain uncertain to about 10 eV in a variety of past experiments, particularly if detuning is used to monochromate the beam, and if direct recalibrations are not performed. The use of powder standards is able to accurately calibrate synchrotron beam line monochromation in the presence of

TABLE II. Energy calibration using the Si 640*b* and LaB_6 powder standards for the energies from the silicon attenuation. The nominal energies (E_{nom}) at which the calibrations were conducted are compared with the calibrated energies using Si 640*b* ($E_{cal,Si}$) and LaB_6 (E_{cal,LaB_6}). $\sigma_{E_{cal,Si}}$ and $\sigma_{E_{cal,LaB_6}}$ are the 1 sd uncertainties corresponding to $E_{cal,Si}$ and E_{cal,LaB_6}, respectively. The calibrated energies using Si 640*b* and LaB_6 powder samples were consistent within uncertainties.

E_{nom} (eV)	$E_{cal,Si}$ (keV)	$\sigma_{E_{cal,Si}}$ (eV)	E_{cal,LaB_6} (keV)	$\sigma_{E_{cal,LaB_6}}$ (eV)	$E_{LaB_6}-E_{Si}$ (eV)	$\sigma_{E_{sum}}$ (eV)
5000			5014.6	1.08		
6000	6010.6	0.57	6011.2	1.56	0.62	1.66
7000	7011.1	1.56	7011.0	0.90	−0.09	2.58
7400	7413.9	0.15	7413.8	0.95	−0.01	1.03
7600	7613.0	0.00	7613.1	0.32	0.06	1.13
8000	8013.5	0.28	8013.6	1.10	0.10	0.82
9000	9013.5	0.28	9015.6	1.09	2.17	1.06
9000	9014.3	0.96	9016.8	0.89	2.50	1.19
10000	10017.1	0.65	10017.5	0.89	0.41	0.70
11000	11020.7	0.87	11020.5	0.82	−0.23	1.14
12000	12020.5	0.90	12021.5	0.99	1.03	1.53
13500	13521.4	0.90	13521.6	0.90	0.28	0.85
15000	15022.8	0.71	15023.6	0.82	0.81	1.61
16200	16225.1	0.47	16225.8	1.04	0.72	1.01
17600	17626.6	1.20	17629.4	0.95	2.82	1.30
18600	18626.9	0.65	18627.3	0.54	0.39	1.31
20000	20027.8	1.39	20028.5	0.81	0.64	1.34

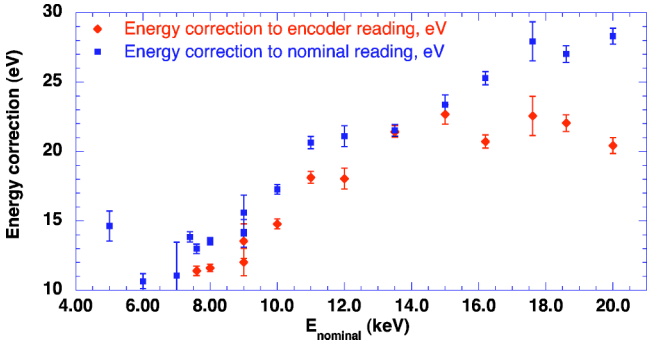

FIG. 5. Energy correction from the silicon experiment derived from weighted mean of the Si and LaB_6 powder standard determinations, applied to nominal monochromator energy and nominal calibrated encoder energies, respectively.

detuning shifts or mechanical hysteresis, for example. We note that, for example, this can be used to recalibrate edge energy determinations which are often used as a secondary standard.

Energy calibrations using the silicon standard are in good agreement on a point-by-point basis with those using the LaB_6 standard within the corresponding uncertainties of the measurement of each standard for individual energies, except at 9 keV and 17.6 eV where the discrepancies are 1.3σ and 1.6σ, respectively.

However, we note that the latter results are typically 10 ± 0.4 eV higher than the former when using the reference lattice spacings of $2d=5.430\,94(1)$ Å for Si 640*b* and $2d=4.156\,95(6)$ Å for LaB_6 660 (Figs. 7 and 8). This discrepancy persists in both experiments, and is of course indicative of an inconsistency in the lattice spacing. The most consistent fit involves a large number of 70 peaks on ten independent image plates for two different powder samples and for this extensive data set has a remarkable associated uncertainty of 0.14 eV.

VI. DETERMINATION OF THE LATTICE SPACING OF LaB_6

The remarkable consistency of the data and the independent determinations of energies argue for the quality of the

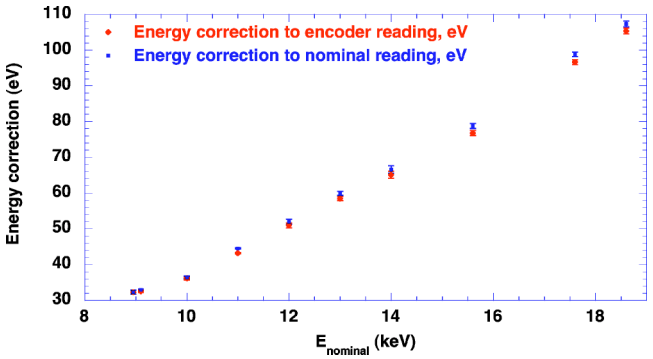

FIG. 6. Energy correction from the copper experiment derived from weighted of the Si and LaB_6 powder standard determinations, applied to nominal monochromator energy and nominal calibrated encoder energies, respectively.

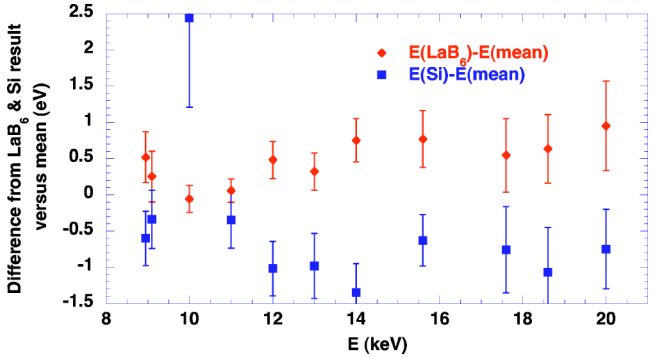

FIG. 7. Systematic discrepancies in the copper experiment between determinations of energy using the Si 640*b* and LaB_6 660 standards.

data and the detail of the investigation. But the correlation of the discrepancy of results using the LaB_6 standard compared to those using the Si 640*b* standard yields a quantifiable determination of the relative lattice spacings of the two standard powders. Subject to correct understanding of absorption, refractive index, and temperature corrections, this yields a measurement of the LaB_6 lattice spacing relative to the Si 640*b* silicon standard.

This systematic discrepancy between the standards is consistent with the lattice spacing uncertainty for LaB_6 **(**$a_0=5.430\,940(11)$ Å [1]**)** corresponding to (3σ) 0.87 eV at 20 keV and 0.39 eV at 9 keV, compared with the 0.12 eV (3σ) uncertainty for the Si standard at 20 keV. However, it also suggests that one of the lattice spacings is different from that reported earlier.

Given the small energy shifts involved, a detailed series of statistical tests was performed to evaluate the significance of the result for subsets which might reveal systematic corrections or shifts to the measured peak location and hence the determined energy.

In particular, the analysis investigated the quantitative correction to the LaB_6 660 lattice spacing afforded by the experimental data, and the ratio of this correction relative to the literature value. Weighted and unweighted mean ratios and standard errors of the means were determined in the usual manner from the data sets, and found to be consistent within cited standard errors for each of the silicon and copper experiments.

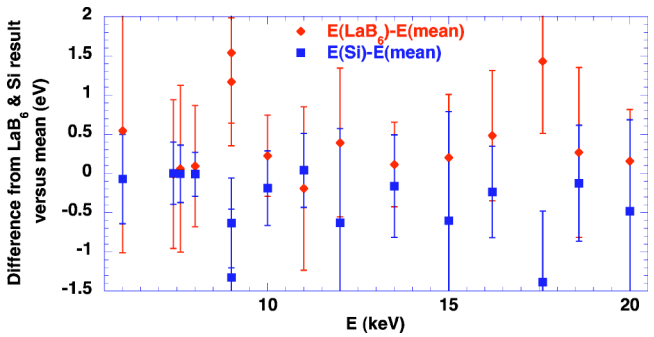

FIG. 8. Systematic discrepancies in the silicon experiment between determinations of energy using the Si 640*b* and LaB_6 660 standards.

A. Correction for temperature

The linear-expansion coefficients of LaB_6 660 (5.42×10^{-6} K^{-1}) and Si 640*b* (2.581×10^{-6} K^{-1}) are significantly different and the lattice spacings have been determined at two different reference temperatures (299 K and 298 K, respectively). Temperatures at the table and at the sample were monitored during the experiments and a 1° variation was observed. Correcting for this at the mean observed temperature of 24.8 °C yields a correction of the relative lattice spacing for LaB_6 660 compared to Si 640*b* of 1.000 005 6 with a similar error ($\pm6\times10^{-6}$). This has the same sign as the observed shift but its magnitude is one order too small to account for the observed systematic discrepancy.

B. Correction for the linearization assumption

The use of Eq. (9) rather than of the nonlinear Eq. (7) can be addressed directly with the results of the fitted parameters and their errors. These have been computed for all peaks and are in general between two and six orders of magnitude smaller than the quoted standard deviations of the individual peak centroid determinations, so have no effect either systematically or statistically on the results.

C. Correction for subset correlations

The analysis fitting all image plates simultaneously was found to give consistent results with the corresponding analysis using individual plate determinations of lattice spacing corrections (or energies) to within one standard error of the corresponding means. Comparison of the "best" data subsets (for example, the 9 keV–20 keV subset of the silicon experiment) provided a result with the same consistency and significance. The separate (copper and silicon) experiments provided lattice spacing corrections again within one standard error of the resulting means.

Many possible systematic errors are temporally dependent, such as, for example, a drift of the energy or monochromator with time after switching to a new energy. In most instances, the LaB_6 660 powder-diffraction pattern was collected before the corresponding Si 640*b* powder-diffraction pattern. The "reverse test" using LaB_6 660 as the second powder determined yielded a result with the same value and significance as the measurements using LaB_6 660 as the first powder investigated for the energies involved (there were three independent tests of this).

Repeated energy measurements allowed the influence of temporal drift to be observed. The "drift test" (the consistency of repeated measurements of either powder under identical conditions) showed no significant drift of either sign with time from six separate measurements.

D. Correction for eccentricity of the powder sample from the central axis of the powder diffractometer

For each powder standard, the influence of any possible anomalous plate was also investigated. The six plates covered the approximate 2θ angular ranges (5°–45°), (5°–85°), (90°–125°), (−5° to −45°), (−50° to −85°), and (−90° to −125°). The symmetry between positive and negative angles was generally very good (and would not influence a shift in apparent energy or lattice spacing) but there was a clear variation of apparent lattice spacing from the low-angle plates to the high-angle plates.

This is direct evidence for a downstream or upstream eccentricity of the location of the powder capillary with respect to the center of the powder diffractometer. This can be due to a physical misalignment of the powder stage or to a nontransparency of the powder at low energies so that (for example) only the front of the powder sample diffracts effectively. With suitable modeling it can be shown that such an eccentricity will (if not determined or corrected for) produce a shift to lower lattice parameters for low angles; and hence that there may be a systematic variation between the results for the two powders due to the nonidentical distribution of powder lines. In particular, LaB_6 generally has more lines at lower angles.

If there is a uniform distribution of peaks determined to similar accuracy across the range of angles above and below 90° or −90°, then an unbiased result would derive from analysis of only the four image plates covering higher angles. This test was also made, which induced a variation in the result of approximately one standard error of the earlier means. Of course this is unsatisfactory, as the distributions are not uniform, and the omission of selected plates will omit data and reduce the statistical significance of the result.

The trend observed was qualitatively consistent with a downstream eccentricity of the powder samples by 0.2 mm compared to the center of the powder diffractometer. While this is quite plausible, the two powder capillaries were aligned (with one another) by an ocular to better than this value, and the capillary diameters of 100 μm imply that transparency corrections and differential offsets were probably an order of magnitude smaller. Hence it is clearly necessary to model directly the eccentricity of the powder capillaries for each powder and energy, and to fit this additional parameter simultaneously with the other variables.

In principle, corrections for lack of centering of the powder sample may be made by fitting the equation

$$\theta = \theta_{meas} + \delta\theta_{offset,plate\ k} + \sin 2\theta \frac{\delta z}{2R} + \cos 2\theta \frac{\delta y}{2R}, \quad (10)$$

where δz and δy are the distances from the powder samples to the center of the diffractometer chamber in the downstream and vertical directions, respectively; and R is the radius of the diffractometer chamber. There was weak indication of any vertical offset, and any such offset would not in fact affect the determination of the relative lattice parameters (or the corresponding energies). In addition, the correlation of this derivative signature with other parameters (especially with the plate offsets) led to this not being fitted in this experiment.

Modeling a downstream offset for individual plates yielded large variability, but modeling a single downstream offset eccentricity for each energy yielded consistent values of 200 μm–300 μm with significantly reduced χ^2 values (typically a reduction in reduced χ^2 of a factor of between 2 and 8). Error and uncertainty estimates were propagated

from the correlations in the full covariance matrix of the fitted parameters. The consistency of the data was improved dramatically by including this single parameter for each powder and each energy. A typical individual standard deviation of the determination of dz was $\sigma_{dz} \simeq 30\ \mu\text{m} - 80\ \mu\text{m}$, so the variation was still significant; but the consistency of the results from different energies yielded an overall uncertainty of the trend of $\approx 10\ \mu\text{m} - 20\ \mu\text{m}$.

The differential shift of the downstream eccentricity between the two powder capillaries is a more important parameter as it could result in a shift in the determined relative lattice spacing. This varied between 10 μm and 100 μm and appeared to be reasonably consistent, with a small trend as a function of energy (which therefore also corrects for a possible transparency). The final mean differential shift was $\approx 10\ \mu\text{m} - 20\ \mu\text{m}$ with a similar uncertainty.

E. Correction for individual anomalous peak centroids

The detailed analysis undertaken allowed individual inconsistencies to be observed. In particular, some individual energies had large error bars for the determined relative lattice spacing correction, and had a variation, for example, of three standard deviations from the determined means. This is to be expected at some level, from purely statistical distributions of outliers. However, such occurrences were investigated and often a particularly extreme outlying peak centroid in a particular plate was responsible. In general this had two possible signatures: usually this was the weakest peak in the particular plate, and was close to the noise level, so that typically the width and amplitude were fitted to local random noise rather than to the true peak. The magnitude of these errors was always less than the half width at half maximum of the peak, so that the peak had indeed been correctly identified and labeled; but the fit was erroneous.

In a couple of instances the peak lay at the very edge of the image plate, and so had in fact been partially truncated, or was the lowest-order reflection and had a large χ_r^2 fitting error due to the profile structure, again leading to a shift of the centroid by up to a half width at half maximum of the peak. Although the peaks were correctly identified and these shifts are quite small and fairly consistent compared to the peak widths, the accuracy of the body of data contained herein allows these points of anomaly to be rejected with much more than a 3σ confidence level. Hence the resulting total data set (of all energies and both powders) was in general only reduced by some 20 individual peaks, but with a much improved consistency of the results.

The traditional literature on powder and single-crystal diffraction is well aware of these problems. Commonly one of a number of standard cutoffs is used on integrated peaks such as the requirement that (integrated) peak intensities be, e.g., three times the corresponding intensity σ or the background noise level. These are useful guides but the best method is based on a statistical determination of inconsistent subsets and hence inconsistent outliers (preferably leading to the physical interpretations outlined above). In all cases these outliers were identified, confirmed by statistical tests, and correlated with one of the clear physical signatures discussed above.

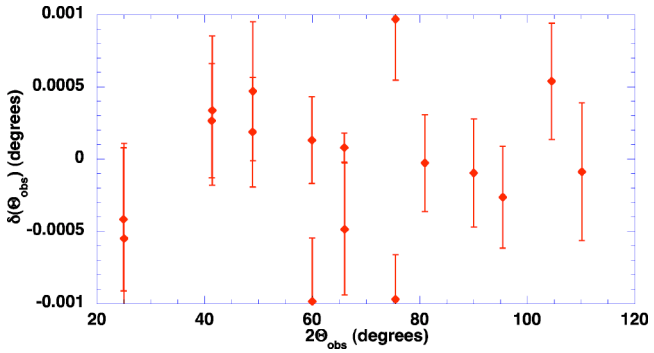

FIG. 9. Standard pattern of angular deviations for a silicon 640*b* powder-diffraction analysis as discussed in the paper. This scan had a relatively small number of peaks, in part because of the use of silicon powder and in part because of the relatively low energy. Nonetheless, the agreement across wide angular ranges to this degree by this technique is remarkable. The average deviation $|\Delta\theta| = 0.00\ 0\ 40°$ is substantially less than the profile widths. Even then, note that the largest deviations are due to the vertical asymmetry of peaks corresponding perhaps to a minor vertical eccentricity of the capillary.

F. Separate and pooled results and discussion

Good determinations of energy corresponded to a mean $|\Delta\theta| = 0.000\ 40° - 0.000\ 48°$, for some 17–77 measured peaks. A total of 2138 peaks were measured for 29 energies or an average of 37 peaks per powder per energy. For the lowest energies (below 8 keV) there were only a few well-determined peaks (3–10) because of the air absorption and exposure times; as can be seen below these consequentially had large uncertainties and did not contribute significantly to the final results.

Standard patterns of angular deviations for the Si 640*b* and the LaB_6 powder-diffraction analyses are presented in Figs. 9 and 10. Most well-presented powder-diffraction analyses provide these sample plots to demonstrate their goodness of fit. Here we additionally present the corresponding error bars on the same plot to emphasize the consistency with the final result.

High-accuracy relative lattice spacing measurements have been made in the past yielding average $|\Delta\theta|$ values for some 85 peaks of as little as 0.001° [21]. This did not lead to an absolute calibration, unfortunately, because there was no absolute reference standard and because the sample observed (Si 640*a*) was sieved so that the lattice spacing did not correspond to the standard. The earlier NBS (NIST) calibration of Si 640*a* using internal tungsten and silver standards (which are not well defined) yielded an average $|\Delta\theta|$ value of 0.002 15° or 0.001 45° after omission of the lowest-order peak [22].

Perhaps the most accurate powder determination was that of Hart *et al.* [23] which included a correction for eccentricity with two parameters, collected very high statistics with narrow profiles, used a more detailed profile function, and returned a value for the lattice spacing of Si 640*b* consistent with the earlier value. With a restricted subset of 12 lines, this achieved consistency to 0.001° or a mean $|\Delta\theta|$ value of 0.0003° excluding the 111 reflection, and confirmed a previous result for Si 640*B* and tungsten powder.

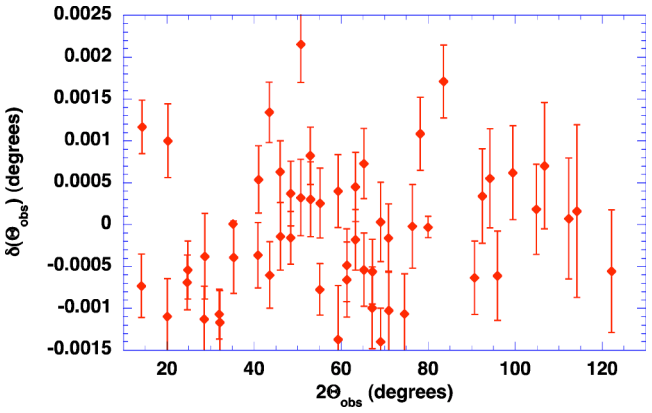

FIG. 10. Standard pattern of angular deviations for a LaB_6 660 powder-diffraction analysis as discussed in the paper. This scan had a relatively large number of peaks, in part because of the use of LaB_6 powder and in part because of the relatively high energy. Nonetheless, the agreement across wide angular ranges to this degree by this technique is remarkable. The average deviation $|\Delta\theta| = 0.0006°$ is somewhat larger than the best data set, but the determination of the fit is just as well defined.

While our data would yield smaller deviations with additional parameters including vertical capillary eccentricity and additional profile parameters, the results we have obtained robustly report $\sigma\sqrt{(\chi_r^2)}$ values and hence we are fairly confident of their reliability in this context.

Figure 11 reports the final consistency of the derived lattice correction ratio for each energy in the first and second experiments, with and without the correction for the downstream eccentricity. Both sets (with and without the *dz* eccentricity parameter) are plotted to illustrate the significant shifts in resulting determinations which can and do occur for particular energies. In most cases the shift is within a standard deviation of either result, but in some cases the shift is two or more standard deviations. The low-energy data (below 8 keV) are affected by the air attenuation in the particular geometry used, leading to relatively few peaks and low significance. Hence the eccentricity is not well determined for the lowest energies, as is reflected by both their increased error bars and by their significant shifts.

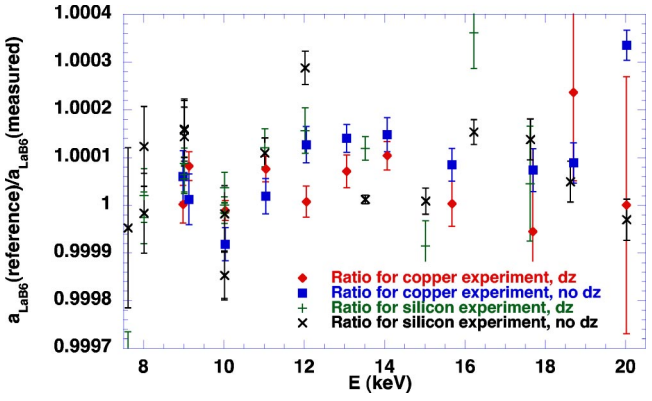

FIG. 11. Plot of the correction ratio for the LaB_6 lattice spacing $a_{reference}/a_{measured}$ for each energy for the two experiments. Values including and excluding the fitting of the downstream eccentricity of the capillary with respect to the diffractometer axis are included. All subsets yield a result consistent to within one standard error of their mean. In most cases, the internal and external consistency of the data has been improved by the details of the text.

At high energies (i.e., 16.2, 18.6, and 20.0 keV) only four plates were used and therefore the determination of the downstream eccentricity yielded large uncertainty and shifts correlated with the uncertainty and value of the parameter *dz*. In these cases the external consistency of the derived lattice spacing shift including a fitting of *dz* is a weak result for these high angles, compared to the result without fitting the parameter *dz*. For example, the fit for the silicon experiment including *dz* for 20 keV yielded a shift in energy of (-8 ± 10) eV for that energy, compared to the result without *dz* of (-0.6 ± 0.9) eV. However, these shifts relative to the final result were of random sign and low significance so that the final results with and without implementation of the eccentricity *dz* were in fact fully consistent within one standard deviation. In general χ_r^2 improved significantly with the introduction of the additional parameter, and this parameter value was consistent and physical, as discussed above.

The weighted mean of the ratios for the copper experiment is then 1.000 041(15); that for the silicon experiment is 1.000 042(19); and the pooled results from both experiments yield 1.000 042(12) or a 3.3 standard error discrepancy from the literature value. Inclusion of the temperature correction yields a correction ratio of 1.000 036 4(140).

Ratios of energies measured using LaB_6 and Si powders yield a relative measurement of the correction for the LaB_6 lattice spacing. The results yield a LaB_6 lattice spacing of $2d = 4.156\ 80(5)$ Å at 299 K instead of the reference value of $2d = 4.156\ 95(6)$ Å.

G. On the refractive index correction for powder diffraction

None of these standards are corrected for refraction in the literature, and therefore our comparison similarly does not include any refractive index correction. It is clear that refractive indices computed from single flat crystal dynamical diffraction theory are quite inappropriate for microscopic crystallites in a powder [24]. Nonideal mosaic diffraction modeling may be used but often has empirical fitting parameters [25]. In the case of powder standards, the computation would need to be carried out for a range of sizes and then require a convolution of the results with the size distribution. Authors have found that the resulting apparent refractive index correction is much closer to zero than the value for a flat single crystal [6]. Hence within the current analysis, there is no correction for refraction.

VII. DISCUSSION OF RESULTS: APPLICATION AND UTILITY

Recently the standards SRM 640*c* and SRM 660*a* have become available and have been analyzed and quantified very carefully [20]. The recent measurements are not published, but include several interesting and applications including a separation of the doublet lines, Soller slits, and a highly accurate goniometer. In general the business of devel-

oping x-ray powder standards has been conducted completely at fixed-source standards laboratories despite individual tests and detailed investigations at synchrotron sources. Often the key problem has been the irreproducibility of the standard, or the measurement at a synchrotron source of a material that is not properly maintained by a corresponding laboratory.

With this result, we demonstrate an approach which is quite manageable for the determination and calibration of numerous secondary standards to high accuracy, with the understanding that development of such experiments would also improve the accuracy and consistency further. In particular, it would seem invaluable to directly investigate the 660*a* and 640*c* standards since the approaches used should be confirmed independently.

A key consequence of this work is that a range of secondary standards could become reliably available for secondary determinations of lattice parameters and also for self-consistent structural investigations, and that direct structural investigations tied carefully to such standards should clearly be able to achieve this stated accuracy and precision in general.

VIII. CONCLUSIONS

A. Accurate powder standard lattice parameters

While it is possible that these results have been due to some change in the samples with time or environment, it is nonetheless surprising that this might have been this large (15σ if it relates to the Si 640*b* standard). Additionally this is a reliable and robust result using the XERT method of investigation, which is able to avoid numerous systematics having some energy dependence, including, for example, the absorption effect. The consistency of these results with energy, combined with the high level of accuracy for each energy, implies that the earlier calibration of LaB_6 NIST SRM 660 was unreliable by several standard deviations, or at least is so now. We therefore provide a calibration of this major standard.

The described technique is quite feasible at major synchrotron facilities and opens the way for the determination of accurate lattice spacings in powder-diffraction analyses of secondary standards and of structures of direct interest relative to the best defined (silicon) standard. We have assessed the advantages and disadvantages of the use of internal standards in a parameter determination only in a qualitative sense. A sequel investigation must, we feel, question this assumption quantitatively, as it is widely used in the literature.

The effect observed is not attributable to temperature changes, positional eccentricities, differential absorption, or any of a wide range of other effects directly investigated. In particular, these results are consistent for the range of energies in measurements where numerous energies were used and hence where differential absorption approaching 0.1 mm might have occurred. The consistency of this result and the cancellation of numerous possible systematic effects by the relative method of comparing results to the Si 640*b* standard strengthens and confirms the result.

B. Energy bandwidth of a monochromated, detuned synchrotron beam

The investigation above shows a clean method for the determination and interpretation of profile widths as a function of angle in terms of the energy bandwidth of the beam. It is likely that the physical basis of the results we have obtained here is a more likely and more commonly observed than any notional dependence upon microstrain, which we believe would normally be masked by the bandwidth. The approach gives a physically plausible magnitude and explains a wide body of data across energies which is not well interpreted on the basis of microstrain or other explanations. Additionally, the x-ray extended range technique allows the partial isolation of some of these key parameters.

C. The lattice spacing of LaB_6 NIST SRM 660 at 299 K

The results lead to a LaB_6 lattice spacing of $2d = 4.156\,80(5)$ Å at 299 K instead of the reference value of $2d = 4.156\,95(6)$ Å. This represents a discrepancy of $\Delta 2d = 0.000\,15$ Å.

This small (3σ) correction is important in the general utility and application of the common powder standards to the wider use of structural evaluation, and this method is able to improve upon the calibrations using fixed sources and highly accurate goniometers at standards laboratories. It must be remembered that single-crystal standards at standards laboratories will remain the key primary standard for x-ray energy determination and lattice parameter determination. The primary standard for powder diffraction at this time must (for the same reason) be determined at such laboratories. However, common and extremely popular secondary standards may then be determined directly at synchrotrons or in carefully calibrated laboratory source arrangements; and in principle either method may yield the accuracy needed for any further calibration or powder investigations.

ACKNOWLEDGMENTS

This work was performed at the Australian National Beamline Facility with support from the Australian Synchrotron Research Program, and was funded by the Commonwealth of Australia under the Major National Research Facilities Program. We thank M. D. de Jonge in general discussions of this research and in careful reading of this manuscript. Associate Professor Zwi Barnea has been a driving force behind this experimental program; and the powder work discussed here has depended critically upon his long experience and insight. We thank him for his critical preparation of the samples, involvement in the experiment and analysis, and careful reading of the manuscript.

[1] W. Parrish, A. J. C. Wilson, and J. I. Langford, in *International Table for X-ray Crystallography*, edited by A. J. C. Wilson and E. Prince (Kluwer Academic, Dordrecht, 1999), Sec. 5.2.10.
[2] A. L. Dragoo, Powder Diffr. **1**, 294 (1986).
[3] J. G. M. van Berkum, G. J. M. Sprong, Th. H. de Keijser, R. Delhez, and E. J. Sonneveld, Powder Diffr. **10**, 129 (1995).
[4] A. M. Glazer, M. Hidaka, and J. Bordas, J. Appl. Crystallogr. **11**, 165 (1978).
[5] T. Nakajima, T. Fukamachi, O. Terasaki, and S. Hosoya, J. Appl. Crystallogr. **9**, 286 (1976).
[6] M. Hart, W. Parrish, M. Bellotto, and G. S. Lim, Acta Crystallogr., Sect. A: Found. Crystallogr. **A44**, 193 (1988).
[7] C. T. Chantler, C. Q. Tran, D. Paterson, D. Cookson, and Z. Barnea, Phys. Lett. A **286**, 338 (2001).
[8] C. Q. Tran, C. T. Chantler, and Z. Barnea, Phys. Rev. Lett. **90**, 257401 (2003).
[9] C. T. Chantler, C. Q. Tran, Z. Barnea, D. Paterson, D. J. Cookson, and D. X. Balaic, Phys. Rev. A **64**, 062506 (2001).
[10] C. Q. Tran, C. T. Chantler, Z. Barnea, D. Paterson, and D. J. Cookson, Phys. Rev. A **67**, 042716 (2003).
[11] P. J. Mohr and B. N. Taylor, Rev. Mod. Phys. **72**, 351 (2000); J. Phys. Chem. Ref. Data **28**, 1731 (1999).
[12] R. D. Deslattes and A. Henins, Phys. Rev. Lett. **31**, 972 (1973); R. D. Deslattes, M. Tanaka, G. L. Greene, A. Henins, and E. G. Kessler, Jr., IEEE Trans. Instrum. Meas. **IM-36**, 166 (1987).
[13] C. T. Chantler, J. Phys. Chem. Ref. Data **22**, 71 (1995).
[14] C. T. Chantler, J. Phys. Chem. Ref. Data **29**, 597 (2000).
[15] G. Materlik and V. O. Kostroun, Rev. Sci. Instrum. **51**, 86 (1980).
[16] Z. Barnea, R. Clapp, D. C. Creagh, T. M. Sabine, A. W. Stevenson, J. W. White, S. W. Wilkins, J. Harada, H. Hashizume, Y. Kashihara, M. Sakata, K. Ohsumi, and T. Zemb, Rev. Sci. Instrum. **60**, 2537 (1989).
[17] Z. Barnea, D. C. Creagh, T. J. Davis, R. F. Garrett, S. Janky, A. W. Stevenson, and S. W. Wilkins, Rev. Sci. Instrum. **63**, 1069 (1992).
[18] T. M. Sabine, B. J. Kennedy, R. F. Garrett, G. J. Foran, and D. J. Cookson, J. Appl. Crystallogr. **28**, 513, (1995).
[19] D. J. Cookson, J. Synchrotron Radiat. **5**, 1375 (1998).
[20] National Institute of Standards and Technology SRM Certificates, Standard Reference Materials 640*b*, 660. S. W. Freiman, N. M. Trahey (and authors J. P. Cline, R. D. Deslattes, J.-L. Staudenmann, E. G. Kessler, L. T. Hudson, A. Henins, R. W. Cheary, J. J. Filiben noted therein) http://www.nist.gov/srm/, 2000.
[21] W. Parrish, M. Hart, T. C. Huang, and M. Bellotto, Adv. X-Ray Anal. **26**, 45 (1983).
[22] C. R. Hubbard, Adv. X-Ray Anal. **30**, 373 (1960).
[23] M. Hart, R. J. Cernik, W. Parrish, and H. Toraya, J. Appl. Crystallogr. **23**, 286 (1990).
[24] C. T. Chantler, J. Appl. Crystallogr. **25**, 694 (1992).
[25] C. T. Chantler and R. D. Deslattes, Rev. Sci. Instrum. **66**, 5123 (1995).